

## MIT Open Access Articles

*Active Yaw Stabilization for Smooth,  
Highly Maneuverable Underwater Vehicles*

The MIT Faculty has made this article openly available. **Please share** how this access benefits you. Your story matters.

**Citation:** Mazumdar, Anirban, et al. "Active Yaw Stabilization for Smooth, Highly Maneuverable Underwater Vehicles." ASME 2012 5th Annual Dynamic Systems and Control Conference joint with the JSME 2012 11th Motion and Vibration Conference, 17-19 October, 2012, Fort Lauderdale, Florida, ASME, 2012, p. 195. © 2012 by ASME.

**As Published:** <http://dx.doi.org/10.1115/DSCC2012-MOVIC2012-8693>

**Publisher:** ASME International

**Persistent URL:** <http://hdl.handle.net/1721.1/118930>

**Version:** Final published version: final published article, as it appeared in a journal, conference proceedings, or other formally published context

**Terms of Use:** Article is made available in accordance with the publisher's policy and may be subject to US copyright law. Please refer to the publisher's site for terms of use.



DSCC2012-MOVIC2012-8693

## ACTIVE YAW STABILIZATION FOR SMOOTH, HIGHLY MANEUVERABLE UNDERWATER VEHICLES

**Anirban Mazumdar**

d'Arbeloff Laboratory for Information Systems and Technology  
 Department of Mechanical Engineering  
 Massachusetts Institute of Technology  
 Cambridge, Massachusetts, 02139  
 Email: amazumda@mit.edu

**Aaron Fittery**

**Martin Lozano**

**H. Harry Asada**

d'Arbeloff Laboratory for Information Systems and Technology  
 Department of Mechanical Engineering  
 Massachusetts Institute of Technology  
 Cambridge, Massachusetts, 02139

### ABSTRACT

*This paper describes the development of a robot that combines a powerful propeller with a pump-valve system that enables high maneuverability. In order to reduce size and improve turning performance, the design does not include external stabilizers such as fins. Therefore the robot is directionally unstable (yaw direction). In this work we outline the design of a linear stabilizing controller that does not require complicated flow sensors and instead simply uses angle and rate measurements. The linear controller was simulated and then implemented on a prototype robot. Preliminary results reveal that this stabilization method works to enable straight motions and is also able to reject substantial disturbances.*

### NOMENCLATURE

$X$  Position in X direction (Earth fixed reference frame).  
 $Y$  Position in Y direction (Earth fixed reference frame).  
 $x$  Position in x direction (vehicle fixed reference frame).  
 $y$  Position in y direction (vehicle fixed reference frame).  
 $z$  Position in z direction (vehicle fixed reference frame).  
 $u$  Surge velocity.  
 $v$  Sway velocity.  
 $w$  Heave velocity.  
 $p$  Roll rate.  
 $q$  Pitch rate.  
 $r$  Yaw rate.  
 $\phi$  Roll angle.  
 $\theta$  Pitch angle.

$\psi$  Yaw angle.  
 $\beta$  Sideslip angle (directional angle of attack).  
 $m$  Mass of vehicle.  
 $I_{xx}$  Centroidal moment of inertia about x axis.  
 $I_{yy}$  Centroidal moment of inertia about y axis.  
 $I_{zz}$  Centroidal moment of inertia about z axis.  
 $X_{prop}$  Force in x direction from propeller.  
 $Y_{J1}$  Force in y direction associated with Pump 1.  
 $Y_{J2}$  Force in y direction associated with Pump 2.  
 $-X_{\dot{u}}$  Added mass associated with translations in surge (x) direction.  
 $-Y_{\dot{v}}$  Added mass associated with translations in sway (y) direction.  
 $-Z_{\dot{w}}$  Added mass associated with translations in heave (z) direction.  
 $-K_{\dot{p}}$  Added inertia associated with rotations about (x) axis.  
 $-M_{\dot{q}}$  Added inertia associated with rotations about (y) axis.  
 $-N_{\dot{r}}$  Added inertia associated with rotations about (z) axis.  
 $-X_{uu}$  Drag force associated with translations in surge (x) direction.  
 $-Y_{vv}$  Drag force associated with translations in sway (y) direction.  
 $-Z_{ww}$  Drag force associated with translations in heave (z) direction.  
 $-K_{pp}$  Drag moment associated with rotations about (x) axis.  
 $-M_{qq}$  Drag moment associated with rotations about (y) axis.  
 $-N_{rr}$  Drag moment associated with rotations about (z) axis.  
 $I_Z$  Total moment of inertia associated with rotations about the z axis.

$M_Y$  Total inertia associated with translations in surge y axis.  
 $\Delta m$  Difference in added masses in y and x directions.  
 $c$  Jet coupling coefficient.  
 $N_M$  Munk moment (xy plane).  
 $N_{Fin,L}$  Moment about the z axis caused by fin lift.  
 $N_{Fin,D}$  Moment about the z axis caused by fin drag.  
 $U_\infty$  Free stream velocity.  
 $U_c$  Cruising speed in surge (x) direction.  
 $K_F$  Force constant for pump-jet system [N/V].  
 $L_F$  x distance between output jet and center of mass.  
 $\gamma$  Stability metric.

## INTRODUCTION

An emerging area in marine robotics is the development of robots that are capable of maneuvering within tight constraints and otherwise cluttered and constrained environments. Examples of such applications include the inspection of water-filled piping structures, evaluation of underwater infrastructure and even the exploration of confined spaces deep underwater. Developing underwater robots that can maneuver at low speeds and in tight spaces is still an emerging area of research. Examples of exciting work include hybrid vehicles based on jellyfish locomotion [1] and vehicles propelled by biologically inspired flapping foils [2].

At MIT's d'Arbeloff Laboratory, work is underway on a new class of underwater robots that combine high performance centrifugal pumps with fluidic valves to achieve multi DOF maneuvering capability. Figure 1 provides an illustration of the type of smooth, highly maneuverable robots currently under development in our group. The vehicle is entirely smooth and symmetric on the outside (with the exception of the propeller in the rear). A pump-jet maneuvering system is located entirely within the shell. Depending on the configuration of the valves and direction of rotation of the pump, the output jet can vary between 4 directions (+y, -y, +z, -z). The 5th DOF, translation in the surge direction (+x, -x) is provided by a propeller in the rear of the vehicle.

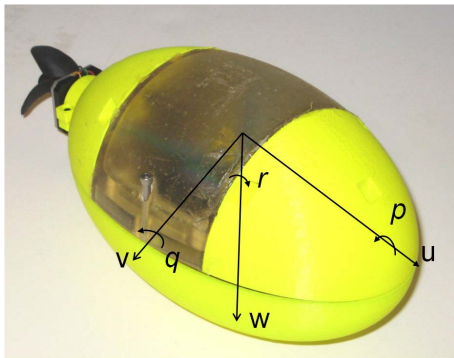


Figure 1. AN ILLUSTRATION OF THE 5DOF, HIGH MANEUVERABILITY ROBOT UNDER DEVELOPMENT AT MIT'S D'ARBELOFF LABORATORY.

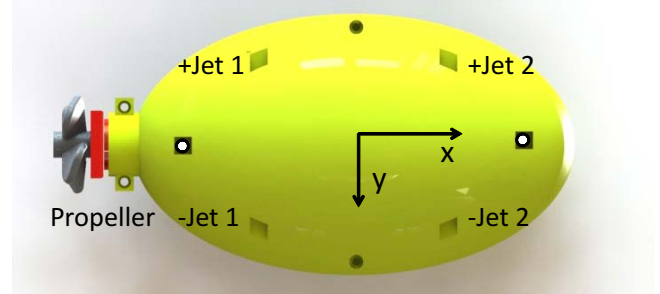


Figure 2. AN ILLUSTRATION OF THE PROPULSION COMPONENTS FOR THE PROTOTYPE ROBOT.

Marine robots in general are designed to be smooth and streamlined for a number of reasons including reduction of drag and ease of control. However, a common challenge with such robots is the presence of the Munk moment which tends to destabilize the vehicle in flow and rotate it to be perpendicular to the flow.

The Munk moment stems from pressure distributions around the ends of the vehicle [3] and is a result of inviscid effects. Viscous effects result in the formation of vortices near the end of the body. These viscous effects tend to stabilize the vehicle to some extent [4]. This effect occurs for both pitch and yaw. However, locating the center of mass below the center of buoyancy is a simple and easy way to passively stabilize the vehicle against pitching moments. This luxury does not exist for yaw. Therefore for the rest of this paper we shall focus on yaw stabilization. If the center of mass and the center of buoyancy are located very close to each other, then the ideas outlined in this paper can also be applied to pitch control.

A closed form expression for the Munk moment exists and is provided in eq. 1. Note that  $Y_v$  and  $X_u$  are both negative, but the absolute value of  $Y_v$  is larger.

$$N_M = U_\infty^2 \cos(\beta) \sin(\beta) (-Y_v + X_u) \quad (1)$$

Expressions for the viscous effects are more difficult to determine as they are reliant on experimental data. A reliable source for such data is [5]. On a qualitative level the text describes how "fatter" bodies of revolution are more unstable and bodies that taper to a point are also the most unstable. Therefore we will assume that the viscous stabilizing effects are small and ignore them for the sake of simplicity.

A common technique for dealing with the Munk moment is to use fins near the tail of the vehicle. The fins create a lift force that is also proportional to  $U_\infty^2$ . If the fins are placed far enough back the moment created by the lift force is enough to cancel out the Munk moment for all speeds. This makes the vehicle passively stable. However, fins can add substantial size and weight. Additionally, in cluttered environments, large fins can snag or collide with obstacles.

In this work we will focus on using our unique pump-valve maneuvering system to provide restoring forces and moments that will counter the Munk moment effect. Previous works have illustrated how the pump-valve system can be used to exploit the high performance of centrifugal pumps and achieve precision closed loop control. Using these maneuvering jets to also achieve stabilization means that no extra hardware such as fins are required for stabilization. For further details on the pump valve maneuvering system refer to [6] and [7].

The remainder of this paper will focus on developing a full maneuvering model and using it to design a control system that can act as a replacement for passive stabilizers such as fins. Linearized models will be used to design the controller, and experimental data will be used to validate this design.

## VEHICLE MANEUVERING MODEL

### Full Model

The full maneuvering model for a 6DOF rigid body vehicle such as an underwater vehicle or an aircraft is complex and nonlinear. An interested reader can refer to a vehicle dynamics course notes such as [8]. We outline several key assumptions that we use to simplify the nonlinear equations.

1. Inertia matrix is assumed to be diagonal (cross terms are zero) due to the symmetric nature of the design.
2. We assume the dominant hydrodynamic forces are from added mass, drag, and Munk moment. Due to the symmetry of the vehicle, added mass and drag cross terms are 0.
3. We assume that the dominant drag is quadratic. This is based on the large Reynolds number ( $\sim 40,000$ ).
4. The center of mass is positioned slightly below the center of buoyancy to provide static pitch and roll stability.
5. Actuator dynamics are sufficiently fast to be neglected from initial analysis.

$$\begin{aligned}
 m \left[ \frac{du}{dt} + qw - rv \right] &= X_{prop} + X_{\dot{u}} \frac{du}{dt} + X_{uu} u |u| \\
 m \left[ \frac{dv}{dt} + ru - pw \right] &= Y_{\dot{v}} \frac{dv}{dt} + Y_{vv} v |v| + Y_{J1} + Y_{J2} \\
 m \left[ \frac{dw}{dt} + pv - qu \right] &= Z_{\dot{w}} \frac{dw}{dt} + Z_{ww} w |w| \\
 I_{xx} \dot{p} + (I_{zz} - I_{yy}) r q &= K_{\dot{p}} \frac{dp}{dt} + K_{pp} p |p| \\
 I_{yy} \dot{q} + (I_{xx} - I_{zz}) p r &= M_{\dot{q}} \frac{dq}{dt} + M_{qq} q |q| \\
 I_{zz} \dot{r} + (I_{yy} - I_{xx}) p q &= (-Y_{J1} + Y_{J2}) L_F + N_{\dot{r}} \frac{dr}{dt} + N_{rr} r |r| + N_M
 \end{aligned} \tag{2}$$

The added mass and drag coefficients were developed using simplified shapes as well as the tables provided in [9]. A simple simulation was performed to verify the validity of the physical model and to illustrate the nature of the instability. The robot was assumed to start from rest and then commanded to move in the  $x$  direction. A small perturbation to the sideslip angle was provided. The simulation results are provided in Fig. 3. Note how the yaw angle slowly increases and then eventually causes the robot to spin. This is due to the robot slowly accelerating until

reaching a speed where the Munk moment becomes substantial. These results qualitatively match our experimental observations.

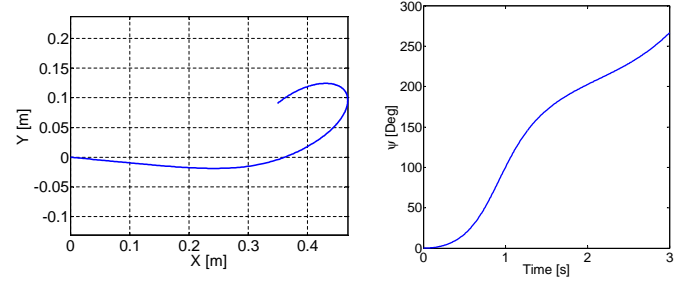


Figure 3. MODEL SIMULATION ILLUSTRATING THE DIRECTIONAL INSTABILITY.

### Linearized Model

While the full governing equations are coupled and nonlinear, linear control techniques are generally a simpler and more intuitive starting point for controller design. We begin by finding the linearized version of the dynamic equations. We linearize about a longitudinal trim state with the vehicle moving with a cruising surge velocity of  $U_c$ . This means that the nominal surge velocity,  $u$ , is set to  $U_c$ . The remainder of the velocities and angles are assumed to be nominally zero. The resulting equations for surge, sway, and yaw are provided. Note that the script  $\Delta$  is used to denote the difference between the linearized result from the full value. Also note that we use a common approximation for the sideslip angle  $\Delta\beta$ .

$$\Delta\beta = \frac{-\Delta v}{U_c} \tag{3}$$

$$(m - X_{\dot{u}}) \frac{d(\Delta u)}{dt} = 2X_{uu} U_c |\Delta u| \tag{4}$$

$$(m - Y_{\dot{v}}) \frac{d(\Delta v)}{dt} = -m U_c \Delta r + \Delta Y_{J1} + \Delta Y_{J2} \tag{5}$$

$$(I_{zz} - N_{\dot{r}}) \frac{d(\Delta r)}{dt} + U_c \Delta v (-Y_{\dot{v}} + X_{\dot{u}}) = (\Delta Y_{J1} - \Delta Y_{J2}) L_F \tag{6}$$

We approximate the pump jet system as a linear system with zero dynamics. We use  $K_F$  to represent the transformation between the voltage input and the force output.

$$Y_i = K_F V_i \quad (7)$$

The planar maneuvering model can be rewritten in state space form where our states consist of  $\Delta v$ ,  $\Delta r$  respectively. We neglect the  $u$  direction because it can be decoupled from the sway-yaw dynamics. Also, since we would like to achieve heading control we include a third state, the yaw angle  $\Delta\psi$ . The inputs to the system will be the control voltages  $\Delta V_1$  and  $\Delta V_2$ . Our output of interest is the heading angle  $\Delta\psi$ .

$$\begin{aligned} \frac{d}{dt} \begin{bmatrix} \Delta v \\ \Delta r \\ \Delta\psi \end{bmatrix} &= \begin{bmatrix} 0 & \frac{-U_c}{m-Y_{\dot{v}}} & 0 \\ \frac{-U_c(-Y_{\dot{v}}+X_{\dot{u}})}{I_{zz}-N_{\dot{r}}} & 0 & 0 \\ 0 & 1 & 0 \end{bmatrix} \begin{bmatrix} \Delta v \\ \Delta r \\ \Delta\psi \end{bmatrix} \\ &+ \begin{bmatrix} \frac{K_F}{m-Y_{\dot{v}}} & \frac{K_F}{m-Y_{\dot{v}}} \\ \frac{-K_F L_F}{I_{zz}-N_{\dot{r}}} & \frac{K_F L_F}{I_{zz}-N_{\dot{r}}} \\ 0 & 0 \end{bmatrix} \begin{bmatrix} \Delta V_1 \\ \Delta V_2 \end{bmatrix} \end{aligned} \quad (8)$$

One thing to immediately note from the state space model is the coupling between the sway velocity,  $v$ , and the yaw angle  $\psi$ . This unusual coupling is a result of the sideslip angle. Note that if there were no jets pointing along the  $y$  direction, the system would be uncontrollable. Many streamlined robots have 2 propeller thrusters at the rear which can provide moments but not sway forces. The ability of our design to provide forces in the  $y$  direction is an unusual feature that in this case is essential for linear control.

## CLOSED LOOP CONTROL

### Linearized Model Response

The most common approach to controller design is to use the aforementioned state space model and incorporate full state feedback. Common techniques would be to use either a Linear Quadratic Regulator (LQR) or a pole placement technique. However, while feedback on  $\psi$  and  $r$  is simple using inertial sensors, measuring  $v$  is harder. Sensors such as pitot tubes can be used, but this adds size, complexity, and can affect the external shape of the robot. Therefore, we will design a controller based only on feedback on  $\psi$  and  $r$ . While this will reduce the performance, it makes implementation much more straightforward. In order to simplify the equations we will use the following simplifications.

$$I_Z = I_{zz} - N_{\dot{r}} \quad (9)$$

$$M_Y = m - Y_{\dot{v}} \quad (10)$$

$$\Delta m = -Y_{\dot{v}} + X_{\dot{u}} \quad (11)$$

Additionally, in order to simplify the controls problem into a single input single output (SISO) system, we will define a variable called the jet coupling coefficient,  $c$ . The jet coupling coefficient is used to relate  $\Delta V_1$  and  $\Delta V_2$ , where  $c$  is a positive number between 0 and 1. The value of  $c$  can be tuned to change the open loop dynamics.

$$\Delta V_2 = -c \Delta V_1 \quad (12)$$

By combining these expressions along with the linear state space model in eq. 8 we can generate a SISO transfer function between the heading angle  $\Delta\psi$  and the jet voltage  $\Delta V_1$ .

$$\frac{\Delta\psi(s)}{\Delta V_1(s)} = \frac{K_F \left( s(-L_F + c L_F) - \frac{\Delta m U_c}{m_Y} (1 + c) \right)}{s \left( I_T s^2 - \frac{\Delta m}{m_Y} U_c^2 \right)} \quad (13)$$

Note how the system has 3 poles, one at the origin, and two symmetrically placed about the imaginary axis. This means that one of the poles is unstable which corresponds with the full nonlinear system. Also note the presence of the zero in the transfer function. By adjusting the value of  $c$  the location of the zero can be changed or eliminated entirely.

We will use parameters that match the physical robot prototype pictured in Fig. 1. The relevant physical parameters are summarized in Table 1. Based on these values, the jet coupling value  $c$  was tuned to be 0.5. This means that the zero is located in the left half of the complex plane at  $s = -0.4$ . Higher values of  $c$  provide greater control authority because it increases the maximum restoring moment that can act on the vehicle.

## Controller Design

An examination of the pole zero diagram of the linearized model reveals that a simple proportional plus derivative (PD) controller could be suitable for stabilizing the system. We begin by placing the zero at  $s = -3.3$ . Note that a negative sign is included in the forward path so that we can still use positive gains. This is a result of our sign convention. We choose the proportional gain based on the saturation limits of the physical system. This ensures that the linear analysis will not break down during actual implementation.

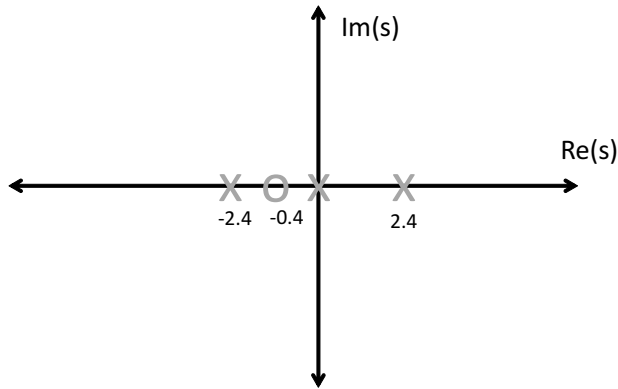


Figure 4. POLE LOCATIONS FOR THE LINEARIZED MODEL.

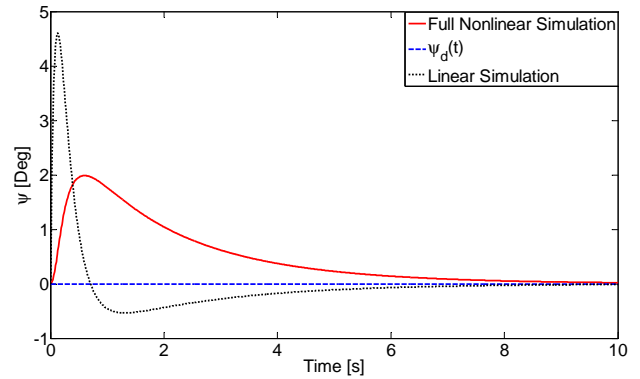


Figure 5. SIMULATED TIME RESPONSE FOR THE LINEAR STABILIZING CONTROLLER.

Table 1. SUMMARY OF PHYSICAL PROPERTIES FOR PROTOTYPE ROBOT.

Parameter	Value
$m$	$0.80[kg]$
$X_{\dot{u}}$	$-0.24[kg]$
$X_{uu}$	$-3.5[kg/m]$
$Y_{\dot{v}}$	$-0.48[kg]$
$Y_{vv}$	$-3.17[kg/m]$
$I_{zz}$	$0.0015[kgm^2]$
$N_{\dot{r}}$	$-0.00015[kgm^2]$
$N_{rr}$	$-0.0006[kgm^2]$
$U_c$	$0.25[m/s]$
$K_F$	$0.0125[N/V]$
$L_F$	$0.038[m]$

The controller performance was evaluated for an initial error in sideslip angle. This models the ability of the vehicle to stabilize itself if it is suddenly disturbed while moving at its cruising speed. As we have already shown, the vehicle without any feedback control immediately sees a divergence in its heading angle. Fig. 5 provides an illustration of the simulated controller response. Note how the controller is able to stabilize the robot in both the linear case as well as for the full nonlinear simulation. In addition, note how nonlinear effects change the controller response. The presence of quadratic drag reduces the overshoot, but the drag and the actuator dynamics also reduce the speed of response slightly.

## IMPROVED PERFORMANCE FROM OPEN LOOP INSTABILITY

There may be cases where directional instability can actually be exploited to improve performance. The use of closed loop control to achieve stability (stability augmentation) can be viewed as having two types of performance benefits. First, the weight and drag of passive stabilizing components can be reduced or eliminated. Second, passively stable designs can act sluggishly when commanded to change position or orientation. Studies on high performance aircraft have illustrated how these improvements can be achieved for Reduced Static Stability (RSS) aircraft. In this section we will discuss how RSS can be used to improve the performance of underwater vehicles.

In the case of underwater robots, the additional weight of fins is negligible as they can usually be made of light or neutrally buoyant materials. Of greater significance is their size. If the fins are too large they can limit the ability of the robot to enter highly confined or cluttered environments. We simulated a tailfin to stabilize the vehicle using a NACA 0015 airfoil. The fin was sized to make the robot only marginally stable. If we assume a simple square geometry, we can easily compute the length of the fin. Our calculations require a fin of a length scale that is nearly 25 percent of the vehicle diameter. These fins can perhaps be placed cleverly so that the net footprint of the vehicle does not change substantially, but the example still reveals that fins can contribute substantially to the size.

In addition, fins result in reduced performance not only due to the restoring force they provide, but also due to the induced drag that occurs at large sideslip angles. The variable  $N_{Fin,L}$  is used to describe the moment provided by lift on the fin. Note that at small angles the drag moment from the fin,  $N_{Fin,D}$  is negligible. The metric  $\gamma$  serves as an intuitive way to describe stability; if there are no fins,  $\gamma = 0$ , and if the fins only achieve marginal stability,  $\gamma = 1$ . Values of  $\gamma$  that are larger than 1 indicate passive stability.

$$\gamma = \frac{N_{Fin,L}}{N_M} \quad (14)$$

### Maneuvering Performance

Several sample NACA 0015 fins were simulated for their ability to make the robot passively stable. Lift and drag data was taken from publicly available tables. While these designs make the robot passively stable, they have other effects on maneuvering performance. A good test of maneuverability is through a “high speed turn test.” In this case the vehicle is moving at a large cruising speed and then tries to turn. The restoring forces and moments of the fins serve to restrict the ability of the vehicle to turn. This effect is illustrated in Fig. 6. Note how the vehicle without fins ( $\gamma = 0$ ) is able to exploit the instability and turn very rapidly compared to the passively stable vehicles.

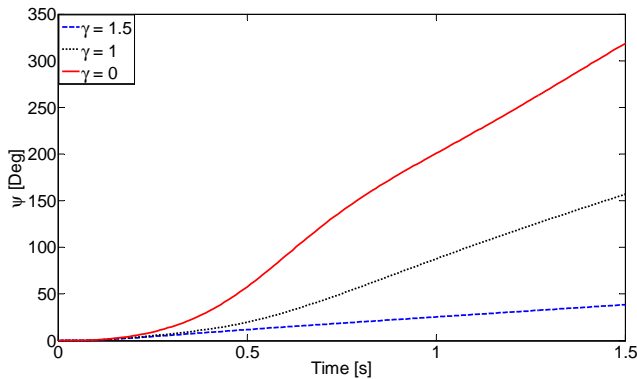


Figure 6. SIMULATION RESULTS FROM THE FAST TURN TEST. RESULTS ARE OPEN LOOP.

Another metric for maneuverability is low speed turning. This involves turning when the vehicle is already at rest. The ability to turn in place is important when moving within complex or confined regions. Underwater vehicles that rely on rudders for maneuvering have difficulty turning in place because the rudder lift force is dependent on forward velocity. The simulated results of a “turn in place test” are provided in Fig. 7. In these tests the passively stable robots do not fare as badly because the lift force is now very small. Note however that the open loop unstable robot still turns faster. This is mainly due to the drag force created by the fins.

### EXPERIMENTAL RESULTS

The prototype described in the introduction of this paper was used to perform some preliminary experimental studies on the techniques discussed in this paper. The robot weighs approximately 800g and is 170cm long. Stabilization using inertial sensors was implemented using a digital inertial measurement unit

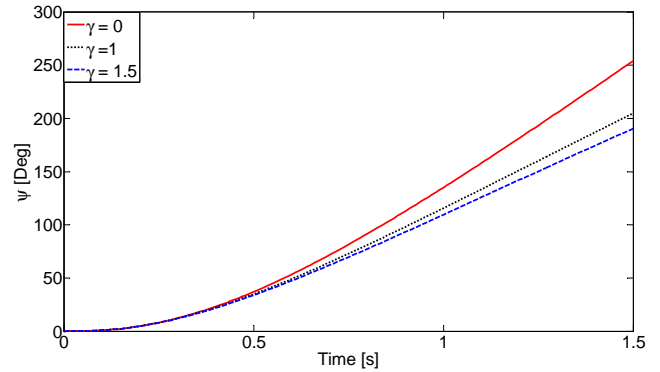


Figure 7. SIMULATION RESULTS FROM THE STATIONARY TURN TEST. RESULTS ARE OPEN LOOP.

that used a gyroscope to estimate both yaw rate and yaw angle. While the integrated gyro does drift slowly, a compass can be used to compensate for this. For these preliminary experiments the time duration was short enough that gyro drift was not an issue. Tests were performed at the ocean engineering teaching facilities at MIT. The controller design technique outlined in previous sections was used to design and implement the closed loop controller. The PD controller zero was placed at  $s = -3.3$ , and the gains match those in the simulation and the jet coupling coefficient,  $c$ , was set to 0.5.

Two basic experiments were performed. First, the feedback controller was implemented and examined for its ability to allow the robot to move straight. The robot forward speed was approximately 0.25 m/s. The results of this experiment are provided Fig. 8. As the data plot shows, the controller stabilizes the forward motion and enables the robot to move straight.

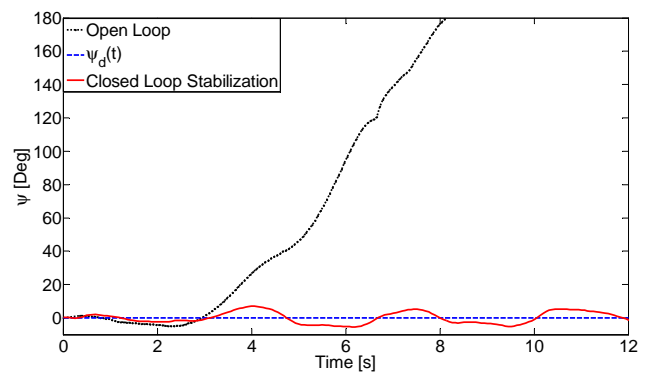


Figure 8. EXPERIMENTAL RESULTS FOR THE STRAIGHT MOTION TEST. NOTE THE CONTRAST BETWEEN THE OPEN LOOP CASE AND THE CLOSED LOOP STABILIZATION.

The second experiment involved disturbance rejection. The robot was commanded to swim straight and then subjected to a



sizable perturbation. The ability of the robot to return to straight motion was examined. An illustration of these results is provided in Fig. 9. Note how the controller is able to respond to a disturbance that turns the vehicle 60 degrees as it is moving at full speed. The controller is able to quickly return the vehicle to straight motion.

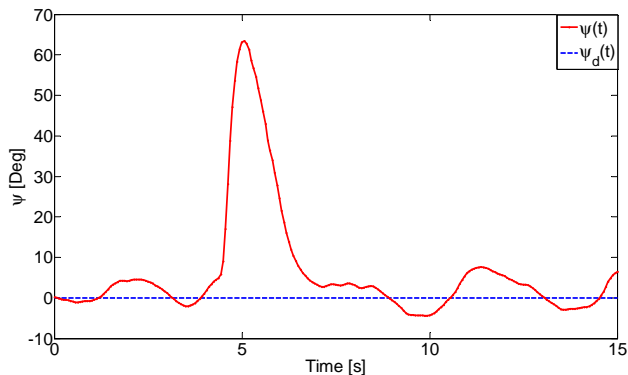


Figure 9. EXPERIMENTAL RESULTS FOR THE DISTURBANCE TEST.

While these results are promising, the vehicle does have low frequency oscillations in its response. One possible source of error relates to the effects of the vehicle pitching up and down near the water surface. This causes the vehicle to bob up and down. Operating at neutral buoyancy in larger tanks is essential to further explore this problem, but for the scope of this paper, the vehicle was allowed to operate very close to the water surface at slightly positive buoyancy. These bobbing motions can sometimes affect the propeller if it is lifted out of the water and can also cause oscillations that affect the controller.

## CONCLUSIONS

This paper describes the development of a novel 5 DOF robot that combines a propellers with pump-valve propulsion in order to achieve both high efficiency and high maneuverability. Due to the Munk moment, the vehicle is directionally unstable. We propose using the pump-valve system to achieve directional stability. Using the internal pump-valve system instead of external fins reduces the size of the vehicle and also has the potential to provide improved turning ability. Models for the robot and instability are outlined, and a linear control system is designed. The linear controller is based on using only angle and rate feedback and therefore avoids the complications associated with measuring sideslip angle or sway velocity. The linear technique was shown to stabilize the vehicle for both linearized models and full nonlinear models that include nonlinear drag, and actuator dynamics. Finally, the linear controller was implemented into the physical prototype with only small adjustments. The controller was shown experimentally to achieve both stable

straight motions as well as substantial disturbance rejection capabilities.

Future work will focus on reducing the low frequency oscillations in the controller response and on improving the controller response so that the vehicle can operate at higher speeds. In addition, the robot requires additional development in order to achieve full 5DOF motions. Exciting areas include high speed maneuvers and incorporating additional sensors for full state feedback.

## ACKNOWLEDGMENT

This material is based upon work supported by the Electric Power Research Institute. In addition, the authors gratefully acknowledge the National Science Foundation's support in the form of a Graduate Research Fellowship. The authors would also like to thank the MIT Energy Initiative for their financial support. Finally, the authors gratefully acknowledge MIT's Bioinstrumentation Laboratory for their assistance in rapid prototyping the physical designs.

## REFERENCES

- [1] Krieg, M., and Mohseni, K., 2010. "Dynamic modeling and control of biologically inspired vortex ring thrusters for underwater robot locomotion". *IEEE Transactions on Robotics*, **26**, pp. 542–554.
- [2] Licht, S., Polidoro, V., Flores, M., Hover, F., and Triantafyllou, M., 2004. "Design and projected performance of a flapping foil auv". *IEEE Journal of Oceanic Engineering*, **29**, pp. 786–794.
- [3] Lewandowski, E., 2004. *The Dynamics of Marine Craft: Maneuvering and Seakeeping*. World Scientific, Singapore.
- [4] Tyagi, A., and Sen, D., 2006. "Technical note: Calculation of transverse hydrodynamic coefficients using computational fluid dynamic approach". *Ocean Engineering*, **33**, pp. 798–809.
- [5] Hoerner, S., and Borst, H., 1985. *Fluid Dynamic Lift*. Mrs. Liselotte A. Hoerner, ch. 19, pp. 1 – 23.
- [6] Mazumdar, A., and Asada, H. H., 2011. "A compact underwater vehicle using high-bandwidth coanda-effect valves for low speed precision maneuvering in cluttered environments". In *Proceedings of the 2011 IEEE International Conference on Robotics and Automation*.
- [7] Mazumdar, A., Lozano, M., Fittery, A., and Asada, H. H., 2012. "A compact, maneuverable, underwater robot for direct inspection of nuclear power piping systems". In *Proceedings of the 2012 IEEE International Conference on Robotics and Automation*.
- [8] Triantafyllou, M., and Hover, F., 2003. *Maneuvering and Control of Marine Vehicles*. See also URL <http://ocw.mit.edu/>, Course 2.154.
- [9] Newman, J., 1977. *Marine Hydrodynamics*. MIT Press, Cambridge, MA.